Biochimica et Biophysica Acta 1797 (2010) 129–142

Contents lists available at ScienceDirect

Biochimica et Biophysica Acta

journal homepage: www.elsevier.com/locate/bbabio

Review

Quantum chemistry as a tool in bioenergetics

Margareta R.A. Blomberg *, Per E.M. Siegbahn

Department of Physics, AlbaNova University Center, and Department of Biochemistry and Biophysics, Arrhenius Laboratory, Stockholm University, SE-106 91, Stockholm, Sweden

ARTICLE INFO

Article history:
Received 9 September 2009
Received in revised form 9 October 2009
Accepted 13 October 2009
Available online 22 October 2009

Keywords:
Quantum chemistry
Cytochrome *c* oxidase
Photosynthesis
Reaction mechanisms
Proton pumping

ABSTRACT

Recent developments of quantum chemical methods have made it possible to tackle crucial questions in bioenergetics. The most important systems, cytochrome *c* oxidase in cellular respiration and photosystem II (PSII) in photosynthesis will here be used as examples to illustrate the power of the quantum chemical tools. One main contribution from quantum chemistry is to put mechanistic suggestions onto an energy scale. Accordingly, free energy profiles can be constructed both for reduction of molecular oxygen in cytochrome *c* oxidase and water oxidation in PSII, including O–O bond cleavage and formation, and also proton pumping in cytochrome *c* oxidase. For the construction of the energy diagrams, the computational results sometimes have to be combined with experimental information, such as reduction potentials and rate constants for individual steps in the reactions.

1. Introduction

The capture, transformation and storage of energy are fundamentally important processes for all living organisms; key examples are photosynthesis and cellular respiration. These are complex processes which for a long time have been extensively studied using all available experimental techniques, including crystallography and a wide range of spectroscopies. Still, many questions concerning these processes remain unresolved. The detailed structure of the oxygen evolving complex (OEC) in photosystem II (PSII) and the mechanism for O–O bond formation are still not known. The most prominent remaining problems in respiration are the mechanisms for proton pumping and O–O bond cleavage. This review will describe how quantum chemistry can contribute to resolve these and other problems in bioenergetics, with photosynthesis and respiration as examples.

The development of quantum chemical methods and models during the last decades has enabled quantum chemistry to make significant contributions to the elucidation of reaction mechanisms in biological systems. In particular, the introduction of gradient corrections in density functional theory (DFT) methods and the construction of so called hybrid methods, such as B3LYP, have made it possible to treat large systems, and specifically large systems containing transition metals, at a high enough accuracy. The modeling of redox active transition metal enzymes using the B3LYP functional started in the middle of the 1990s, using active site models containing 20–50 atoms. Today models with about 150 atoms are routinely used to study enzyme mechanisms. For more limited investigations even models with more than 200 atoms can be used.

One type of application of quantum chemistry in biochemical research is in the search for atomistic descriptions of the mechanisms for enzymatic reactions, where chemical bonds are cleaved and formed. Such mechanisms are often suggested on the basis of crystal structures or other experimental information, although mostly with limited possibilities to judge their thermodynamic or kinetic feasibilities. Using quantum chemical calculations on models of the active site, the energetics of different reaction mechanisms can be scrutinized, and suggested mechanisms can be confirmed or rejected based on the calculated energetics. Obviously, new mechanisms can also be suggested based on the results from quantum chemical model calculations. Two examples of this kind of unresolved reaction mechanisms are the O–O bond cleavage step in the terminal respiratory enzyme cytochrome *c* oxidase, and the O–O bond formation step in photosynthesis, which will both be discussed below.

To set up active site models for quantum chemical studies of enzymatic reaction mechanisms, an X-ray structure is used as a starting point. Without a reasonably well-resolved crystal structure, the modeling becomes much more uncertain. However, quantum chemical calculations can also contribute to the resolution of intricate structural problems. An example of this is the oxygen evolving complex (OEC) in PSII, which contains four manganese centers, and due to the low resolution of the PSII X-ray structure the details of the manganese cluster cannot be determined. As will be shown below, results from quantum chemical calculations can be used to obtain an improved structure of the manganese complex. Another structural aspect that is usually not well determined from crystallography is the protonation state of certain residues. Here, quantum chemical calculations on different protonation states assessing the effects on the energetics of different reaction steps can help to determine the most likely protonation states.

* Corresponding author. Tel.: +46 8 16 12 64.
E-mail address: mb@fysik.su.se (M.R.A. Blomberg).

0005-2728/$ – see front matter © 2009 Elsevier B.V. All rights reserved.
doi:10.1016/j.bbabio.2009.10.004

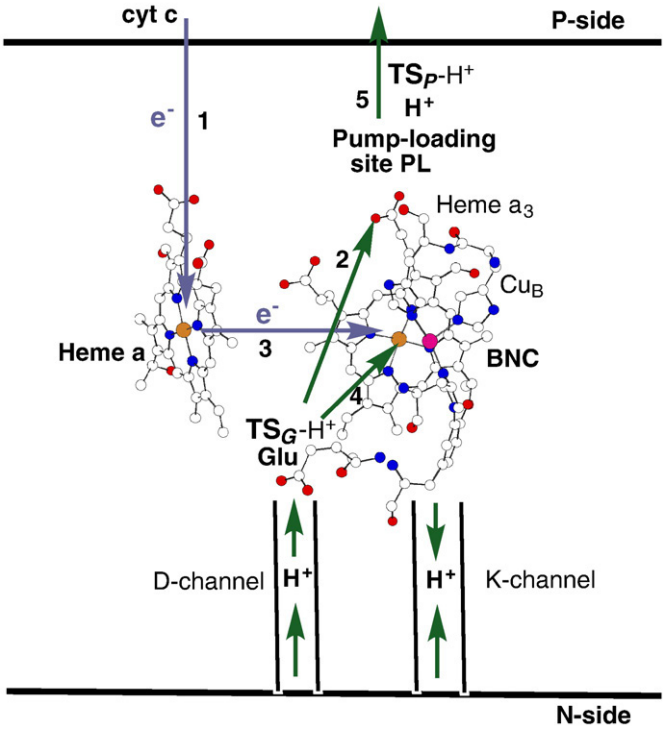

Fig. 1. Schematic picture of electron and proton flow in cytochrome *c* oxidase.

In many biochemical reactions, electrons and protons enter or leave the active site during the catalytic reaction. To determine the energetics for such reactions, redox potentials and pK_a values of donors and acceptors have to be compared. It is difficult to determine such properties with high accuracy theoretically. The main reason is that there are, besides quantum chemical difficulties, also large environmental effects on properties involving a change in charge. For acceptors and donors in different environment calculated values will often not have comparable accuracy. Therefore, another approach has been developed, where only the relative values for a single site are compared at different steps of the catalytic cycle, and the external acceptor or donor is parametrized using experimental redox potentials. This procedure is applied both for water oxidation in photosynthesis and O_2 reduction in respiration, as will be discussed below. The overall exergonicities for these two processes are taken from experimental values, while the individual steps in the catalytic cycle are determined by quantum chemical calculations.

Finally, to determine the mechanisms for proton pumping in the terminal respiratory enzyme, the energetics for proton motion over a large part of the enzyme has to be described. It is not possible to construct reasonably small models for quantum chemical calculations of these processes. Instead, another approach has been developed, where the normal quantum chemical tool of constructing energy profiles is used in conjunction with experimental information, in particular kinetic measurements. This methodology will also be described below.

2. Cytochrome *c* oxidase

Cytochrome *c* oxidase, the terminal respiratory enzyme, has four redox active metal centra, see Fig. 1. Two of them are used for electron transport only, these are a dinuclear copper center, Cu_A (near cytochrome c, not shown), and a low-spin heme, heme a. The other two metal centra form a binuclear center (BNC) where the O_2 chemistry occurs, and the BNC consists of another heme group, heme a_3 and a copper complex, Cu_B.

The reduction of one O_2 molecule can be written:

$$O_2 + 8H_N^+ + 4e^- \rightarrow 2H_2O + 4H_P^+$$

The four electrons are delivered via a cytochrome *c* on the P-side of the mitochondrial membrane, and the four protons needed to form the water molecules in the BNC are taken up from the N-side of the membrane, via two proton channels, labeled the D- and the K-channel (see Fig. 1). Coupled to this exergonic reaction, another four protons are pumped across the entire membrane, from the N-side to the P-side. Both the chemistry and the proton pumping contribute to the build up of an electrochemical gradient, in this way efficiently storing the energy, to be used by ATP-synthase making ATP. As mentioned above, quantum chemical methodology can be used to study both the chemistry of the catalytic cycle, including the O–O bond cleavage and the mechanism for proton pumping. The quantum chemical calculations discussed below are performed on models of the binuclear iron-copper center starting from one of the crystal structures and using the hybrid DFT functional B3LYP. A few atoms on the edge of the model are fixed to their positions in the experimental structure when different intermediates are optimized. The polarizing effect of the surrounding protein is included as a homogeneous dielectric medium with a dielectric constant of 4.

2.1. Mechanism for O–O bond cleavage in cytochrome oxidase

Molecular oxygen coordinates reversibly to the reduced binuclear center (BNC), Fe(II)-Cu(I), giving rise to the observed intermediate labeled compound A, see Fig. 2. The next observed intermediate is labeled P, since it was first thought to be a peroxide. Experiments on the fully reduced form of the enzyme, i.e. where also Cu_A and heme a are reduced, soon showed that the O–O bond is actually cleaved in the P intermediate, labeled P_R in this case. To cleave the O–O bond in molecular oxygen, four electrons are needed. The BNC can provide three of these, resulting in the oxidized Cu(II) and Fe(IV), and in the fully reduced enzyme the fourth electron is given by heme a. Experiments were also made on the mixed valence form of the enzyme, i.e. with only the BNC reduced, and Cu_A and heme a oxidized, which is considered to be the form that actually occurs during the catalytic cycle in the active enzyme. The question was if the O–O bond is cleaved also in the P-type of intermediate formed in the mixed valence enzyme, labeled P_M. It was suggested that the fourth electron could be provided by a near-by amino acid, e.g. the tyrosine that had recently been found to be covalently cross-linked to one of the histidine ligands of Cu_B.

Early calculations on models of the binuclear center were performed to evaluate if it is energetically feasible to form an O–O bond cleavage product in the mixed valence form of the enzyme,

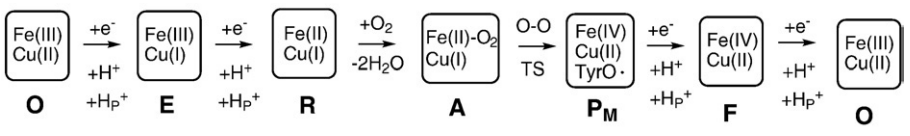

Fig. 2. Sketch of the catalytic cycle in cytochrome *c* oxidase. H_p^+ represents protons pumped across the membrane.

taking the fourth electron from the tyrosine. This appeared as an attractive type of problem for a quantum chemical study since it could be considered as a normal chemical reaction occurring in a closed system, with no electrons entering or leaving the active site during this reaction step. It had furthermore been experimentally established that no protons are taken up or expelled by the enzyme during this step. The first models used in the calculations had only 55 atoms [1,2], still including all the essential parts of the BNC. Using this small model, it could be shown that the O–O bond cleavage reaction forming Fe(IV) = O, Cu(II)-OH and a neutral tyrosyl radical is thermodynamically feasible. However, the calculated barrier for the O–O bond cleavage step was much too high, at least 25 kcal/mol, compared to the experimental value of 12.5 kcal/mol as obtained from the lifetime of compound A and transition state theory [3]. It was at that time suggested that an extra proton might be available in some part of the BNC, and it was shown that such a proton would lower the barrier enough to make the reaction kinetically feasible. In parallel to the calculations, it was shown experimentally that the O–O bond is indeed cleaved in the mixed valence enzyme, and what still remains is to determine the mechanism for the bond cleavage.

A few questions can be raised about the early calculations. First, the models used can be considered as too small and unrealistic, and therefore the results might be unreliable. Therefore, several new calculations have been performed using larger and more realistic models [4–6]. As will be discussed below, the results of the larger models point in the same direction as the first small model calculations, the calculated barrier is significantly higher than the experimental one. Second, the addition of an extra proton in the BNC might not be in accordance with the pK_a values in the vicinity of the active site. Clearly, to just add a proton to the active site, as was done in the first calculations, is a too simplified modeling, and better models for changing the charge in the active site will be described below. Finally, the suggested mechanism assumes that the tyrosine proton moves to the molecular oxygen coordinating to the heme iron during the bond cleaving reaction, and to make this possible, water molecules have to be added to the active site. It is not clear what are the best positions for such water molecules, and if the water molecules in the BNC are unbound relative to bulk water, the cost of moving the waters to the BNC has to be included. Fortunately, a new X-ray structure of the fully reduced cytochrome oxidase was recently determined, which has several water molecules present in the active site [7]. This new structure has been used to construct a new model of the BNC, which is used in calculations on the O–O bond cleavage step. Preliminary results from these calculations will be used below to furthermore demonstrate the different difficulties encountered in the description of the O–O bond cleavage step.

The new model of the BNC used to study the O–O bond cleavage step is shown in Fig. 3. The main amino acids at the BNC are truncated at the alpha carbons, except for the adjacent His333 and His334 where the backbone between them is kept. The heme group is modeled by an unsubstituted porphyrin except that the farnesyl hydroxyl and the formyl groups are kept. The X-ray structure contains four water molecules at the BNC for the reduced state, one of the water molecules is substituted with the oxygen molecule and the other three are included in the model. Two amino acids hydrogen bonding to the water molecules are modeled in a simple way, just to include the hydrogen bonding. This leads to a model of compound A with 144 atoms. Some atoms are fixed at their positions in the crystal structure to keep some strain from the protein, see Fig. 3. In compound A, the oxygen molecule is reduced to a superoxide by one electron from iron, giving Fe(III) with low-spin coupling. The unpaired electrons on dioxygen and iron are anti-ferromagnetically coupled to an open shell singlet.

The O–O bond cleavage occurs in two steps, in the first step the tyrosyl proton is transferred the distal oxygen, and at the same time an electron is transferred to the oxygen to give a FeOOH peroxide. This

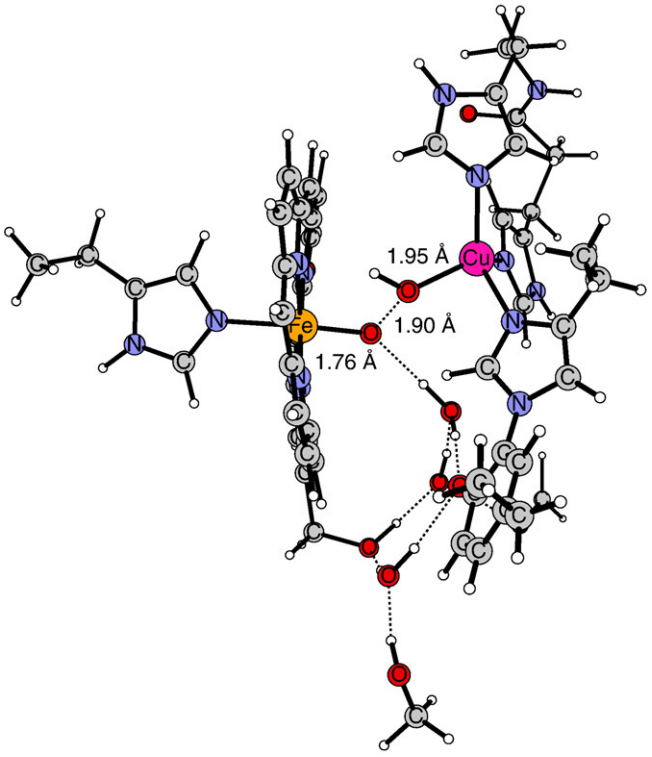

Fig. 3. Structure of the optimized transition state for the O–O bond cleavage in cytochrome *c* oxidase.

electron is taken from Cu_B or the tyrosine, depending on the model and the exact structure of the FeOOH moity. In the second step, the O–O bond is cleaved, and another electron is transferred to the oxygen, giving the Fe(IV) = O, Cu(II) OH, TyrO product. As mentioned above, the lifetime of compound A corresponds to a total free energy of activation of 12.5 kcal/mol. However, the weak temperature dependence of the rate of P_M formation indicates that there is a large entropy effect on the activation energy of 6.1 kcal/mol, yielding an enthalpy barrier of only 6.4 kcal/mol [3]. Thus, if the interpretation of these experiments is correct, the directly calculated activation energy, which corresponds to the enthalpy of activation, should be compared to the lower value of 6.3 kcal/mol, and the entropy effect should be added on top of this. Using the present model already the first step, the formation of an FeOOH peroxide, is found to be endothermic by 9.8 kcal/mol. The barrier for this step has not been definitely determined, but an approximate value is 16 kcal/mol relative to compound A. On top of this endothermicity, the O–O bond cleavage barrier is found to be 11.2 kcal/mol, resulting in a total enthalpy barrier of 21 kcal/mol, as compared to the experimental value of 6.3 kcal/mol. The same two steps have been investigated previously with several models, differing in the number of water molecules present, the exact modeling of the amino acids and the porphyrin with substituents, but with the same protonation states of the included amino acids, and similar results were obtained with all models. The endothermicity of the first step varies between 8 and 13 kcal/mol, and the barrier for the O–O step varies between 8 and 12 kcal/mol (relative to the peroxide). One of these models include the heme propionates with their hydrogen bonding units, and this model therefore has a different total charge than the rest of the models. Still the results are quite similar. Thus, reasonably large models, including all aspects of the binuclear center that are expected to be important, give calculated enthalpy barriers between 16 and 24 kcal/mol compared to the experimental 6.3 kcal/mol.

As mentioned above, the addition of an extra proton to the active site was found to lower the activation energy for the O–O bond

cleavage. The most likely site for an extra proton in the vicinity of the BNC is Lys362 in the K-channel. On the basis of electrostatic calculations, it has been claimed that this lysine is neutral [8,9], but there are experimental indications that it might be protonated [10]. A protonated Lys362 would electrostatically stabilize a negatively charged tyrosinate and thereby the formation of the FeOOH intermediate. In contrast to the mechanism studied in the early quantum chemical, calculations such a proton should not participate in the chemistry at the BNC. From the distance between Lys362 and Tyr288 (13 Å), a stabilization energy of 5–6 kcal/mol can be estimated (using $\varepsilon = 4$). A larger stabilization would be obtained if the lysine proton is allowed to move closer to the tyrosine when the tyrosine proton moves towards the dioxygen. However, since the peroxide state is not observed experimentally, the free energy of the peroxide must be about 3 kcal/mol above compound A. It can be noted that if there is an entropy effect on the activation energy for the O–O bond cleavage, it is most likely to occur between compound A with a loosely bound oxygen molecule and the more firmly bound peroxide FeOOH. Using the experimentally determined entropy effect of about 6 kcal/mol, it means that to give a free energy endothermicity of 3 kcal/mol, the enthalpy of the peroxide should be about 3 kcal/mol below that of compound A instead of the calculated 9.8 kcal/mol above, indicating a stabilization of about 13 kcal/mol from a proton in the K-channel. This corresponds to moving the proton from the Lys362 about half of the way closer to the Tyr288. At the same time, the calculations show that a proton in the K-channel does not change the O–O bond cleavage barrier relative to the peroxide state. Assuming such a strong stabilization of the FeOOH peroxide state, placing its free energy 3 kcal/mol above compound A, and using the presently calculated O–O cleavage barrier of 11.2 kcal/mol gives a total free energy barrier for the A to P_M step of 14.2 kcal/mol in good agreement with the experimental value of 12.5 kcal/mol.

Other ways to lower the O–O bond cleavage barrier, apart from an extra proton in the K-channel, has also been investigated. In the same way as a positive charge near the tyrosinate can stabilize the FeOOH peroxide, a negative charge near the peroxide proton could have a similar stabilizing effect. This might be achieved by deprotonation of one of the histidine ligands on Cu_B. Therefore, calculations were performed with the above described model, just deprotonating His334. As expected, this leads to a stabilization of the FeOOH peroxide, but only by 6.5 kcal/mol relative to compound A, yielding an endothermicity of 3.3 kcal/mol for this step. The O–O bond cleavage barrier calculated from the peroxide is found to be 12.0 kcal/mol in this model, thus essentially unchanged by the deprotonation of the histidine. As is clear from the discussion above, the stabilization obtained in this way is not enough to reach agreement with the experimental barrier since a stabilizing effect twice as large is needed. A completely different way to solve the problem with the endergonicity of the A to FeOOH peroxide step is to abandon the suggestion that the tyrosine proton is used to form the peroxide [6]. The peroxide proton could come from the D-channel, like several protons do in later steps of the catalytic cycle, and the tyrosine proton could leave into the K-channel to allow for the formation of a neutral tyrosyl radical. The motion of two protons in opposite directions would cancel each other and not be observable in electrogenic measurements. Therefore, such a mechanism would be in agreement with the experimental observation that the O–O bond cleavage step is not associated with significant proton motion perpendicular to the membrane. The energetics of this kind of mechanism cannot be estimated, it can only be postulated that the peroxide formation would have to be endergonic by about 3 kcal/mol, to give agreement with the experimental rate of P_M formation.

To make it possible to transfer the tyrosyl proton to molecular oxygen, as suggested in the original mechanism, at least one or two water molecules had to be added to the BNC, which in earlier X-ray structures did not contain any water. The binding energy of those water molecules can be calculated and compared to their binding energy in bulk water. A standard value for the binding energy of one water molecule in bulk water is 14 kcal/mol, and if the calculated binding energy in the BNC is less than 14 kcal/mol, the difference has to be added as a cost to the relative energy of the proton transfer process. A difficulty here is to find the optimal number and positions of the added water molecules since the DFT-optimization procedure used does not guarantee that global minima are found. In the earlier calculations, the water molecules were positioned in the simplest possible way to aid the proton transport, and as was later found, using more appropriate larger models [11], those water molecules were significantly unbound with respect to bulk water. As also mentioned above, the new structure for the reduced state [7] contains several water molecules, and the uncertain positioning of water molecules can be avoided. This also gives a possibility to calibrate the calculations of the water binding energies in the BNC. Using the present computational approach, the water molecules present in the crystal structure of the BNC are found to be bound by about 12 kcal/mol. This network of water molecules can be used to transfer the proton from the tyrosine to O_2, and therefore no extra cost needs to be added for the water molecules in the calculations above on the O–O bond cleavage step.

2.2. Mechanism for proton pumping in cytochrome oxidase

As shown in Fig. 2, the O_2 reduction occurs in four steps. In each step, an electron and a proton is taken up to the BNC for the chemistry, and one proton is pumped from the N-side to the P-side. To understand the pumping mechanism implies an understanding of how these different parts of a reduction step are organized and how the protons are governed to move in the desired directions. Different mechanisms for proton pumping have been suggested, and several of them can be summarized into a standard model for the organization of the steps as follows, see also Fig. 1. In step 1, an electron is transferred from cytochrome *c* to heme a. This raises the pK_a value of a pump-loading site (PL) in the vicinity of the active site, where the protons to be pumped are temporarily stored during the transfer across the membrane. In step 2, a proton is taken up from the N-side via the D-channel to the PL-site. It is not known exactly where the PL-site is, but a common suggestion is one of the propionates of heme a_3. In step 3, the electron is transferred from heme a to the BNC and in step 4 the chemistry is completed by the uptake of a proton from the N-side to the BNC. At this point, the pK_a of the PL-site is back to its lower value and the pump-proton is expelled to the P-side of the membrane in step 5. Essentially the same procedure occurs four times, one for each electron, with the main variation that in one or two steps the K-channel is used instead of the D-channel for the chemical proton. This scheme has been described as a mechanistic model for proton pumping based on electroneutrality and electrostatic repulsion. It should be noted, however, that there is no directionality in this model, there is nothing that prevents the protons to be taken up from the P-side of the membrane instead of the N-side, and there is nothing that prevents the pump-protons to be expelled back to the N-side when they are repelled by the chemical proton. Some kind of gating is needed.

In the beginning of the pumping process, with only a small membrane gradient, a thermodynamic gating might be possible, but not when the gradient increases. Therefore, some type of kinetic gating is needed, and to describe that type of gating transition states need to be introduced. At least two transition states are needed, one between the P-side of the membrane and the PL-site, labeled TS_P in Fig. 1, and one in the D-channel, labeled TS_G in Fig. 1, here assumed to be located at or near the Glu278 at the end of the D-channel. TS_P has to be high enough to prevent protons from entering from the P-side and low enough to allow the pump-protons to pass when they are expelled to the P-side. TS_G on the other hand has to be low enough to allow the protons to enter from the N-side to both the PL-site and the

BNC but also high enough to prevent back flow from the PL-site when the chemistry is completed and the pump-proton should be expelled to the P-site. A thorough analysis of a recent kinetic experiment [12] for one of the reduction steps (O to E, see Fig. 2) made it possible to construct an energy diagram that can fully explain the gating mechanisms in the sense that allowed reaction pathways, i.e. leading to both chemistry and pumping, at all branching points have lower barriers than the forbidden reaction paths not leading to pumping [11,13]. As it turns out, the most intricate transition state to describe is TS_G, and as will be discussed below, the only way to make it possible to prevent back flow of protons from the PL-site to the N-side is to assume that this transition state can have a positive character. It is known from experiment that Glu278 has a high pK_a value, and it is therefore normally protonated. A positively charged transition state for proton transfer from the N-side of the membrane to the PL-site could occur in such a way that the GluOH proton starts to move towards the PL-site when a proton from the N-side is already close to the Glu. The $GluO^-$ therefore becomes immediately reprotonated. It has been suggested that a rotational isomerization of the Glu may present an alternative to the positively charged transition state for the prevention of proton backflux [14]. As will be discussed below the suggested rotation of the Glu does not prevent proton leakage when the chemistry is completed.

The gating mechanism using a positively charged transition state to prevent the protons at the PL-site to leak back to the N-side, rather than being pumped out to the P-side, when the chemistry is completed is illustrated in Fig. 4. The boxes describe different states during one reduction step and the five substeps discussed above are also indicated. One important state is shown in box c, where the electron on heme a stabilizes a positively charged TS_G, allowing the proton to enter from the N-side to the PL-site with a low barrier. At this point, TS_P is higher in energy than TS_G, preventing protons to enter from the P-side. The next important state is shown in box f, showing that when there is no negative charge near TS_G this barrier will be high, preventing the back flow of the protons at the PL-site. At this stage, the TS_P barrier is lower than the TS_G barrier, allowing the protons to be pumped. Fig. 5 shows the energy profiles for a proton moving between the N-side of the membrane and the PL-site. The energy profiles and the discussion here concern the situation with no electrochemical gradient over the membrane. In this situation the transfer of a proton from the N-side to the PL-site is exergonic by 5 kcal/mol when an electron is present on heme a, as derived from

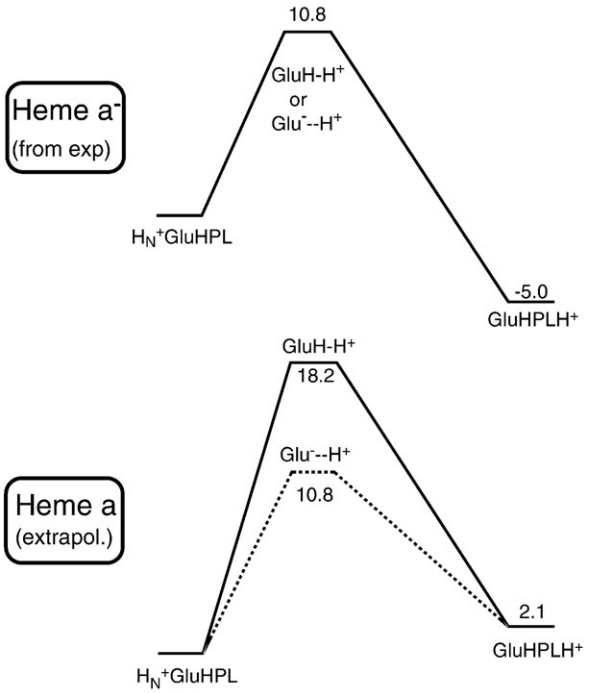

Fig. 5. Energy profiles for proton transfer between the N-side of the membrane (H_N^+) and the pump-loading site (PL) assuming a one-step reaction. The lower profiles illustrate two different extremes for the character of the one-step TS: the full curve corresponds to a positively charged TS, and the dotted curve corresponds to a neutral charge separation type of TS.

kinetic experiments [11-13]. When the chemistry is completed in BNC, i.e. with no uncompensated negative charge in the vicinity, the same step is endergonic by 2 kcal/mol [11,13]. The energy profiles in Fig. 5 are based on the assumption that the proton transfer from the N-side to the PL-site is a one-step process as described above. As shown in the top profile in Fig. 5, when heme a is reduced the barrier will be low, allowing a proton from the N-side to be taken up to the PL-site. A barrier of 10.8 kcal/mol is determined from the experimentally observed rate for this step of proton uptake, using transition state theory. When the electron is neutralized by the chemical proton arriving at the BNC, the positively charged TS is raised by approx-

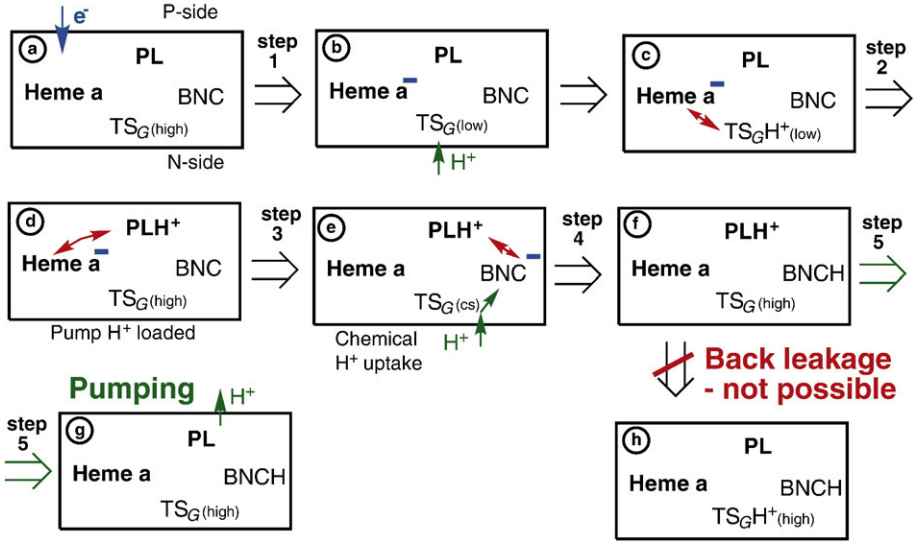

Fig. 4. Scheme for the proton pumping, highlighting the electrostatic mechanism for gating protons toward the P-side of the membrane. The red arrows indicate a mutual electrostatic stabilization.

imately the same energy as the PL-site and the barrier becomes high in energy (18.2–2.1 = 16.1 kcal/mol), preventing back leakage of the proton at the PL-site to the N-side, as illustrated by the lower profile in Fig. 5 read from right to left (full line curve). On the other hand, if the proton from the N-side does not immediately reprotonate the $GluO^-$, a proton transfer with a neutral, charge-separated TS is obtained, still in a one-step process with two protons moving concertedly. This type of TS will not be affected by a negative charge in the vicinity, and the low transition state involved in the proton uptake from the N-side to the PL-site (upper profile in Fig. 5) will be even lower (10.8–2.1 = 8.7 kcal/mol) for the back flow of protons from the PL-site when the chemistry is completed, as illustrated by the dotted curve in the lower part of Fig. 5 (read from right to left.) The conclusion from this analysis is that a positively charged transition state for proton transfer between the N-side and the PL-site is needed to prevent back leakage of protons to the N-side rather than pumping to the P-side.

An alternative type of gating than the one proposed here has been suggested in the so called water-gated mechanism [15,16]. That mechanism and the one described above have one important point in common, which is that an electron on heme a controls the gating. The main difference is that in the water-gated mechanism, there is a coupling between the electron on heme a and water dipoles, while in the above scheme there is a coupling to a positively charged TS. The distance between heme a and Glu278, which is in the critical TS region, is 13.6 Å. The energetic effect of coupling an electron on heme a to a positive charge on Glu278 is then 7.4 kcal/mol using a dielectric constant of 3.3 as derived from the kinetic experiments [13]. The effect is precisely enough (the minimal effect required) to lead to gating. The corresponding coupling effect from an electron on heme a, obtained similarly, to a water molecule in the vicinity of Glu278 with a dipole moment of 1.85 D is only 0.2 kcal/mol. It therefore seems that, even if many water molecules are involved, the coupling effect in the water-gated mechanism would not be enough for gating. On the other hand, lining up the water molecules is most probably needed for allowing the proton to reach the pump site or the BNC.

It can easily be understood that a coupling effect from the electron on heme a of at least 6 kcal/mol is needed for gating even in the general case, if a reasonable efficiency of 99% should be achieved. With the electron on heme a, a rate for proton transfer with a barrier at least 3 kcal/mol *lower* than the rate-limiting step of the entire process is needed to allow 99% efficiency for moving the protons to the PLS. On the other hand, without the electron on heme a, a rate with a barrier at least 3 kcal/mol *higher* than the rate-limiting barrier is required to prevent the backflow from being larger than 1%. The reason a coupling effect of 7.4 kcal/mol is needed in practice has to do with other details [13].

It could be argued that the assumption of a one-step proton transfer between the N-side and the PL-site assumed in the discussion above is too simplified, and that another conclusion might be drawn if a more complicated two-step process is considered. As will be described below, this is not the case, and the same conclusion is therefore drawn for a two-step procedure. A two-step process is often assumed for the protonation of the BNC, where the Glu278 proton first goes to the BNC, and after a Glu^-BNCH intermediate has been formed, the Glu^- is reprotonated from the N-side. An energy diagram for this reaction step is sketched in Fig. 6, where the experimental rate is used to determine the rate-limiting barrier to be 13.2 kcal/mol. To construct this energy profile, it is assumed that the second step, the reprotonation of the Glu^- is fast and not rate limiting. This is based on the simple argument that if the reprotonation of the Glu^- from the N-side was slow, there is a risk that the Glu^- is reprotonated from the PL-site which is protonated at this stage, thereby destroying the pumping. It has been suggested that a mechanism for making this reprotonation barrier from the N-side low, is a fast rotation of the Glu side chain [14,17,18]. Clearly, if the Glu side chain has to rotate to deliver the protons, it is likely that the back rotation should be fast. However, it is

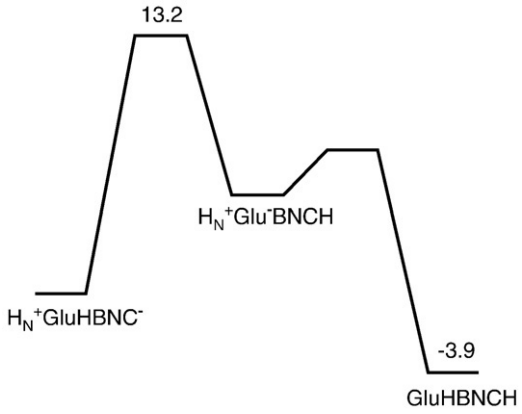

Fig. 6. Energy profile for the reaction step where a proton is taken up from N-side of the membrane (H_N^+) to the BNC, assuming a two-step process where the GluOH proton first goes to the BNC, and the reprotonation of the Glu^- occurs in a second step.

also possible to keep the reprotonation barrier low without the involvement of a rotation of the side chain. Similar to the BNC-protonation process, a two-step process for the proton transfer between the N-side and the PL-site can be constructed. Fig. 7 shows energy profiles for a two-step process where the GluOH proton first goes all the way to the PL-site giving the intermediate, labeled H_N+Glu^-PLH+, the energy of which is here placed at +6.3 kcal/mol, based on the estimated pK_a difference of the Glu278 and the PL-site. The transition state for this step is labeled TS_{PL}. In a second step the Glu^- is reprotonated from the N-side, with a transition state labeled TS_N. The upper profile in Fig. 7 corresponds to the situation observed experimentally with an electron present in heme a, and where the rate-limiting barrier is determined to be 10.8 kcal/mol. From the experimental observations, it cannot be directly concluded which of these two barriers is rate limiting. However, as discussed above in connection with protonation of the BNC, it is clear that the reprotonation of the Glu^- from the N-side has to be fast, and therefore only the case with TS_{PL} rate limiting is considered. The effects on the two-step energy profile from removing the electron on heme a (corresponding to completing the chemistry in the BNC) can be

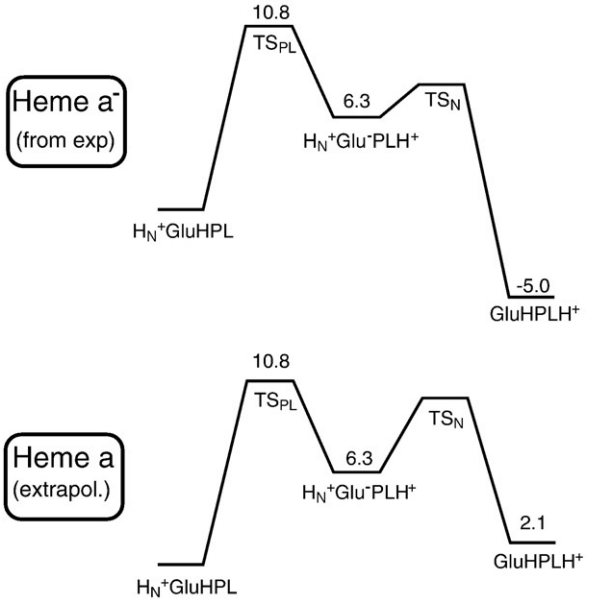

Fig. 7. Energy profiles for proton transfer between the N-side of the membrane (H_N^+) and the PL-site assuming a non-concerted, two-step reaction with charge separation occurring at the glutamate (GluH).

evaluated by estimating the effects on the end point and the intermediate. As above, for the one-step profile, the final point with GluHPLH+ is raised by 7.1 kcal/mol due to the decreased pK_a value of the PL-site. The same raising effect applies to the intermediate, since the PL-site is fully protonated also here. For the intermediate, on the other hand, the absence of the heme a electron has a stabilizing effect on the negatively charged Glu^-. It is here for simplicity assumed that these two effects are of the same size, implying that the energy of the intermediate is unchanged. The energy of TS_{PL} will be unchanged by the removal of the heme a electron, since this transition state is neutral, while the energy of TS_N will be raised due to the decrease of the pK_a value of the PL-site. For simplicity, it is assumed that the TS_N will be raised by 3.5 kcal/mol, which is the average of the effects on the two limiting states of this TS. The right-hand side in the lower profile in Fig. 7 now corresponds to the situation when the chemistry is completed and there is a proton at the PL-site. Reading this profile from right to left shows that the barrier for back leakage to the N-side is too low (10.8–2.1 = 8.7 kcal/mol), just as for the one-step process assuming a charge separation type of TS. The conclusion is the same as before, there has to be a positively charged transition state to prevent back leakage to the N-side. As mentioned above, it has been suggested that the Glu residue can work as a valve and prevent proton back leakage by a fast rotation, and that this may be an alternative to the positively charged transition state discussed here [14,17,18]. However, it can be noted that the suggested fast rotation of the Glu side chain is only a mechanism for keeping the TS_N barrier low, and it does not affect the rate-limiting TS_{PL}. Therefore, the Glu rotation does not prevent proton back leakage when the chemistry is completed and the proton in the PL-site should be pumped to the P-side.

A few comments on the above discussion have to be made. There is an uncertainty about how much the energy of TS_N is raised when the heme a electron is removed. This depends on the exact position of the proton at the transition state structure. However, TS_N can never be higher than TS_{PL} since this would lead to a non-allowed situation with leakage during the Glu^- reprotonation after protonation of the BNC, as discussed above. It follows from the above conclusion that a two-step procedure with neutral transition states can never prevent back flow of the pump-protons when the chemistry is completed. It can also be noted that if TS_N is very low, the two-step energy profile approaches the one-step concerted profile with a neutral transition state discussed above.

The lower energy profile in Fig. 7 can furthermore be used to reject the argument that the proton cannot leak back from the PL-site to the N-side, due to the fact that the GluOH proton is blocking this pathway [19,20]. As is clear from this profile, reading it from right to left, the GluOH proton can easily be moved away to the N-side with a low barrier and a reasonably low endergonicity, and from that point, the barrier for moving the PL-proton to the Glu is low.

2.3. Energetics of the catalytic cycle in cytochrome oxidase

Almost all the processes in cytochrome oxidase can be described as proton or electron transfer reactions. To determine the energetics of these processes, one needs to know pK_a values and redox potentials of different sites at different points of the catalytic cycle. In principle, both pK_a values and redox potentials can be calculated by quantum chemical methods. However, relative energies for processes where the charge is changing are highly dependent on the environment, and it is therefore difficult to construct models that give reliable absolute pK_a values or redox potentials. Quantum chemical methods can also be used in combination with electrostatic methods, which has been done, e.g. to evaluate pK_a values of possible pump-loading sites [21–23] but the results differ between different approaches by more than 10 pK_a units for the same site at the same stage of reduction, showing that this is a very difficult task.

A limited but important goal is to describe the total energy change of each of the four steps in the catalytic cycle described in Fig. 2. Each step involves the uptake of one electron (from cytochrome *c*) and one proton (from bulk water on the N-side), plus the translocation of one proton from the N-side to the P-side of the membrane. Starting with the situation before the electrochemical gradient has begun to build up, there is no cost of the proton translocation. The total cost for the uptake of the electron and proton is identical in all four steps, thus there is only one unknown parameter, corresponding to the uptake of a hydrogen atom (a proton and an electron), and each step can be considered as the formation of a new O–H bond. Using a model of the BNC (including the cross-linked tyrosine), the O–H bond strength of each of the four steps in the catalytic cycle can be calculated, and since there is no change in charge for the uptake of a hydrogen atom, this bond strength is much less dependent on the environment than the pK_a value and redox potential. Furthermore, only the relative bond strengths are needed since the cost for the uptake of the hydrogen atom is the same for all steps. This type of calculations should give a rather good picture of the relative energetics for the four different steps. Finally, by a simple parameterization, the calculations can be made to reproduce the experimental total exergonicity of one cycle, corresponding to the difference in redox potential between the donor (cytochrome *c*) and the ultimate acceptor (molecular oxygen). Using experimental redox potentials and considering that four electrons are involved, this energy gain is 51 kcal/mol [24]. A preliminary energy diagram constructed in this way using the model in Fig. 3 is shown as the lower, full line curve in Fig. 8. Similar diagrams have been constructed earlier, using somewhat different models of the BNC for

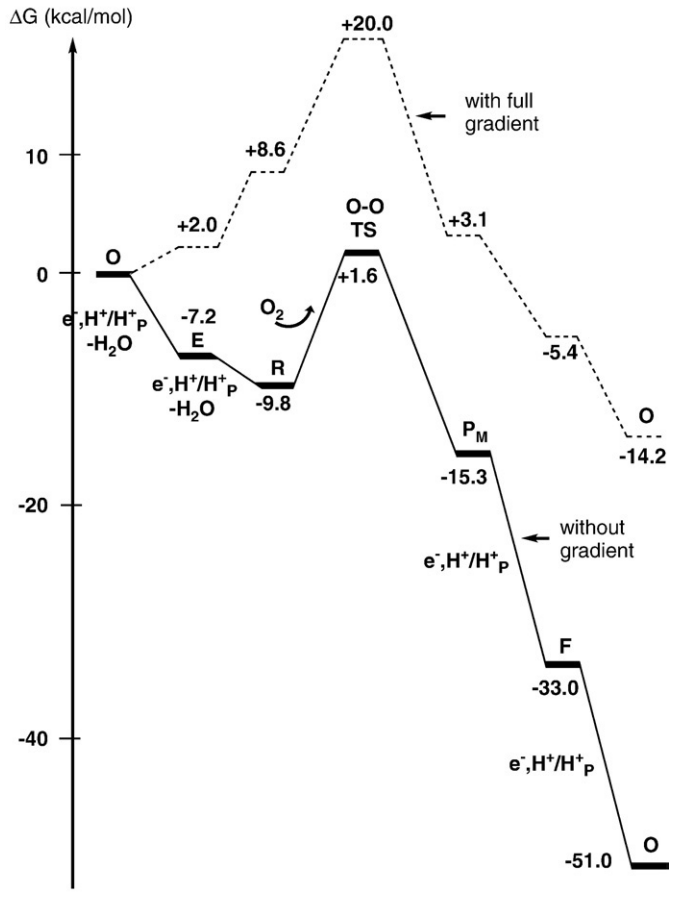

Fig. 8. Energy diagram for dioxygen reduction in cytochrome *c* oxidase showing the transitions where both an electron and a proton have been taken up. H_p^+ indicates that a proton is pumped across the entire membrane. The energies have been parametrized to give an overall energy of 51 kcal/mol. Tyrosinate is assumed to be present until the R-state.

the quantum chemical calculations and slightly more complicated parameterization procedures trying to describe the energetics more in detail, the first one published in 2003 [5,6,25,26]. The general picture obtained from all the different models is the same, the energy release is significantly smaller in the reductive part of the cycle (O to R) than in the oxidative part (P to O), indicating that the energy release from the chemistry in the reductive part might be too low to afford pumping of one proton per electron in this part. There is experimental evidence for the pumping of one proton per electron in the entire catalytic cycle, at least without electrochemical gradient. Ideally, all four steps should have about the same exergonicity, since the low exergonicity in some of the steps makes it difficult to construct a common pumping mechanism for all steps.

Starting from the calculated energy profile described above, the effect on the energetics of the presence of an electrochemical gradient can easily be evaluated. Since each of the four steps in the catalytic cycle corresponds to moving two charges against the gradient, and it is known from experiment that the maximum gradient is about 200 mV [24], an energy profile shown as the upper, dashed curve in Fig. 8 is obtained for the situation with full gradient. From this diagram, it can be seen that both steps in the reductive part of the cycle (O to E and E to R) become endergonic with full gradient, as indicated above. One possibility to decrease this endergonicity would be that when the gradient increases the pumping in these two steps ceases. It is, however, not trivial to construct a pumping mechanism where the pumping ceases due to a too low exergonicity, while the chemistry still occurs. Therefore, it seems most likely to assume that these calculations do not give a completely correct picture of the energetics. In a previous study [6], the results were improved in this respect by the introduction of a correction for the Fe(II) energy, based on a possible DFT error for the spin splittings of this state. A DFT problem could be part of the explanation, but since also the experimental redox potentials for the resting enzyme point in the same direction as the calculations [27], it is likely that there is a problem with the description of the reaction steps. Some aspect of the active site in CcO is probably not taken into account, neither in the redox titrations on the resting enzyme nor in the theoretical modeling. Therefore, new calculations are performed using different models, searching for a better way to describe the chemistry that occurs in the BNC. The models used are varied in different ways, both in terms of size and total charge of the system. It should in this context also be noted that the picture given above where each step is considered as a formation of a new O–H bond is somewhat too simplified, since the electron and the proton are not necessarily going to the same part of the BNC. Therefore, the energetics of the different reaction steps is most likely somewhat more dependent on the description of the surrounding than expected for a simple O–H bond formation.

Another important question, related to the discussion above on the energetics of different steps in the catalytic cycle, is which position in the active site is protonated in each step. The protonation pattern in the BNC can have implications for the pumping mechanism, and it might also explain the existence of two proton channels, the D- and the K-channel between the N-side and the BNC. The protonation sites are not so easily determined experimentally but are rather straightforward to investigate theoretically. The calculations show that for several steps in the catalytic cycle there are two protonation sites with similar pK_a values, the tyrosinate formed when the P_M state is reduced and one of the oxygen coordinating to the metals. Using the present model, the O-state has about the same energy for the two protonation sites, while for the E-state protonation of the tyrosinate is about 5 kcal/mol more favorable. The calculations also indicate that if the protonation occurs at the tyrosine, the relative electron affinity of the BNC will not be raised as much as if the central BNC is protonated, and it will therefore be very low compared to the electron donor, causing a too high barrier for the following electron transfer. Therefore, in the energy profiles in Fig. 8, the tyrosinate is left unprotonated until the last step where the R-state is formed. On the other hand, with water molecules present within the BNC, as in the most recent crystal structure [7], it might be possible for the proton to move relatively freely between the different sites. The barriers for this type of proton transfer are under investigation for the new model with the positions of the BNC water molecules determined by the crystal structure. If it is too easy for the protons to move within the active site it will be more difficult to explain the presence and role of the two proton channels.

There are very few other attempts to calculate the energetics of the entire catalytic cycle of cytochrome oxidase. In one study, published in 2007 [28], the same energy steps as illustrated in Fig. 8 were investigated using the same methodology (DFT with the B3LYP functional) and a similar model of the active site. Still the results are rather different, in the sense that the exergonicity of the two parts of the cycle, the oxidative and the reductive part, are much more similar. The parameterization of the cost of the uptake of the proton and the electron is also different, which, however, does not affect the partitioning of the energy between different steps. Another significant difference between the results from that study and the present one is that the tyrosinate form (protonation of a metal bound oxygen) of the O-state was found to be about 15 kcal/mol lower in energy than the tyrosine form, while in the present study the energy of the two forms is very similar as mentioned above. It was suggested [28] that these two forms of state O should correspond to the resting and the working form observed experimentally. The most likely explanation to the differences between the results of Ref. [28] and the present ones is that for certain intermediates, the calculations in Ref. [28] have converged to excited states, which is indicated by the relative energies given in Table I in Ref. [28]. Another study trying to put the entire catalytic cycle of cytochrome oxidase on an energy basis was published in 2008 by Fee and coworkers [29]. The latter study, which is also a DFT study (different functionals) using similar models as the present ones, goes into great details and tries to describe all individual steps including the proton pumping. The approach is, however, very different from the present one, and it is therefore not possible to compare the results. It can be noted, though, that the energy diagrams published in Fig. 6 in Ref. [29] involve too high thermodynamic barriers to be compatible with the reaction rate of the enzyme. Finally, a very early attempt to calculate part of the catalytic cycle of cytochrome oxidase, the O to E and E to R steps, was published in 2000 [30]. However, the use of small models and methods with low accuracy (Hartree-Fock) prevented any conclusions about the energetics of these steps.

Spectroscopic methods have been applied to elucidate the more detailed structure of different intermediates in the catalytic cycle of cytochrome oxidase, see for example [31-33]. In this context, quantum chemical vibrational analysis of model complexes can help the interpretation of experimental results [34,35]. The role of the tyrosine cross-link has also been addressed by quantum chemical calculations [36,37], and finally a few quantum chemical calculations have been made trying to investigate one of the proposed proton pathways [38].

3. Water oxidation in photosynthesis

Water oxidation in photosystem II proceeds in a sequence of four S-transitions from S_0 to S_4, in which the oxygen evolving complex (OEC) is oxidized four times. Parallel to these oxidations, two substrate water molecules are deprotonated. At the final S_4-state, the O–O bond is formed and O_2 is released. To understand water oxidation therefore means understanding, all the S-state transitions involved and finally the mechanism for the O–O bond formation. Ideally, the starting point for the calculations would have been a high resolution X-ray structure for at least one of these S-states. Since the

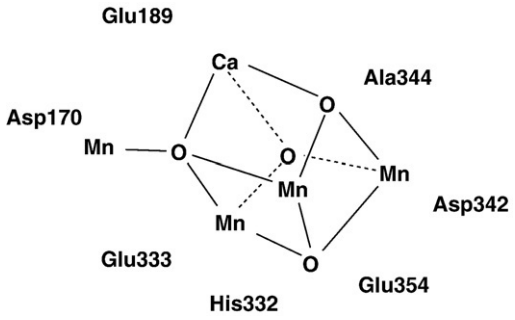

Fig. 9. Simplified picture of the structure of the oxygen evolving complex, suggested by X-ray crystallography [39]. In the more recent structure [40], the manganese outside the cube is further out.

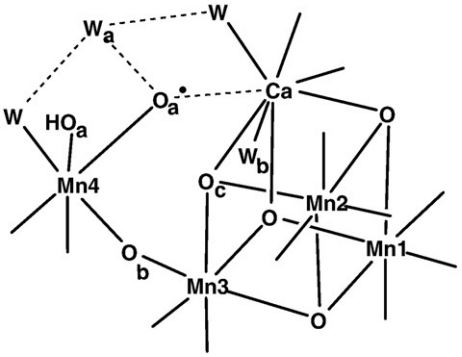

Fig. 10. Schematic picture of the S_4-state of the oxygen evolving complex showing the labeling of the manganese atoms and the relevant oxygens.

only available X-ray structures have rather low resolution of 2.9–3.5 Å [39-41] and the structures furthermore could be affected by X-ray damage [42], other approaches to this problem have been needed.

The manganese cluster obtained from the X-ray investigations is schematically shown in Fig. 9. The reason only a schematic picture is shown is that the exact ligation to the metal atoms had to be partly assumed and is quite different in the two X-ray structures. In the London X-ray structure [39], the binding of the carboxylate amino acid ligands (aspartates and glutamates) was assumed to be mostly monodentate to one metal. In contrast, in the Berlin X-ray structure [40,41], most of these ligands were assumed to be bridging between two different metals. Possibilities in between these two types of ligations are also possible. The ligands that directly bind to the manganese atoms are Asp170, Glu189, His332, Glu333, Asp342, Ala344 (a peptide terminal carboxylate ligand) and Glu354.

3.1. The structure of the oxygen evolving complex

With the lack of an X-ray structure, the first years of DFT studies of water oxidation were spent trying to find the general principles for O–O bond formation using rather crude models [43,44]. The main conclusion from those studies was that O–O bond formation with a low barrier requires a manganese bound oxygen radical. As the first X-ray structures appeared, more realistic models of the OEC could be used. Still, in the first studies of the type discussed here, the models were rather approximate and contained only 50–80 atoms, all described quantum mechanically without enzyme constraints. The directly bound ligands of the OEC and the second shell Arg357 were usually included in the models. The ligand structure had to be assumed and was taken as a mixture of the London and Berlin assignments. The procedure used, which will here be termed the cluster approach, focuses on energy minimization of different reaction pathways. This type of approach for enzymes in general has recently been reviewed [45]. Parallel to those studies, a different DFT approach to water oxidation was used by another group [46]. In that approach, the entire enzyme was modeled using QM/MM (quantum mechanics/molecular mechanics). A small QM part was surrounded by a large MM part, together making up the entire protein. The starting point was the London structure and one of the goals was to match theoretical and experimental spectroscopic data. Entirely different results for both structures and mechanism were obtained with these approaches, as will be described below.

The earliest attempts to model water oxidation by models mimicking the X-ray structures finally led to an optimal S_4 structure with an oxygen radical bound to the external manganese, see Fig. 10. An important step toward a low-barrier mechanism for O–O bond formation was taken when essentially all possibilities to form the O–O bond with the oxygen radical were investigated for this S_4 structure [47]. Rather surprisingly, the by far lowest barrier was found for a reaction between the oxygen radical and a bridging oxo-group. Until then, the lowest barrier found was always one where the oxygen radical is attacked by an outside water [43], but the barrier for that mechanism was already known to be far too high. What was even more surprising in the new mechanism was a spin requirement for a low barrier, see Fig. 11. This requirement means that all spins on the four most directly interacting atoms have to be alternating. The two oxygens O_a and O_c have to have opposite spins to form a bond, and the manganese binding these atoms, Mn4 and Mn2, have to have opposite spins to the respective oxygen. The reasons for the requirements on the manganese spins are in one case a formation of the reduced Mn (III) in a high-spin state and in the other case to allow O–O bond formation without crossing to another spin-surface. It should be added that later studies instead placed the oxygen radical in the Mn_3Ca-cube, at the O_c position, and the oxo-group is then a bridging oxygen to the outer manganese [48,49]. The spin requirement with these new positions is identical to the old one.

The studies described above were all designed in attempts to find the explicit mechanism for O–O bond formation. Until then, the cluster approach had not seriously been used trying to find a structure of the OEC better than that provided by the low-resolution X-ray analysis. For that purpose, a different approach, still built on the results reached above, was employed. It was concluded that the most important structure obtained so far from the calculations was that of the S_4-state where the O–O bond is formed, see above [47]. Attempts to fit the structures of this S_4-state (with an oxygen radical and a low barrier) to the X-ray structure were therefore first made. The cluster models used included the same amino acids as before, but now the full

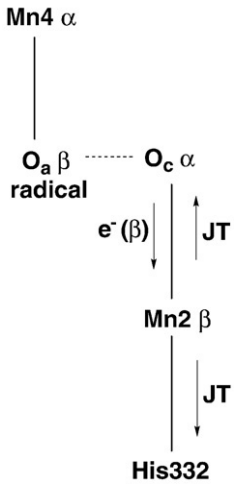

Fig. 11. Requirements for a low O–O bond formation barrier. α and β denote spin directions.

amino acids were described, including the backbone atoms. An important assumption was made at this stage. It was first concluded that the most accurate positions determined by the X-ray analysis are the positions of the backbone atoms. Their positions are, for example, rather close in the two X-ray structures even though the OEC metal complexes are quite different [39,40]. The assumption made was therefore that these positions are sufficiently well described by the low-resolution X-ray structures, that a further optimization of the structure is meaningful. To ensure that the optimized models stayed as closely as possible to the X-ray structures, the backbone atoms were therefore fixed at the positions given by the X-ray structure (taken from the London analysis). This meant that 20 atoms, of a total of about 130, were fixed, while the rest were optimized. With this approach, a search for a better OEC-cluster was initiated. Still, there are a very large number of possibilities, so only the chemically most reasonable ones were fully investigated. Another underlying assumption in this context should be emphasized. Based on experience during the past decade, it was assumed that the lowest energy structure obtained in this way, with the backbone constraints, is the one that is adopted by nature. Against this assumption, it can be argued that it is in principle possible that a higher energy structure is used in the enzyme, if the barriers for its decay are high enough, but this is here considered as very unlikely (see further below).

It turned out that it was relatively easy to make the S_4-state, obtained in the earlier studies, to fit into the backbone structure given by the X-ray analysis [50]. In fact, this protein fitted structure gives an even lower barrier than before for O–O bond formation. However, to obtain a more direct comparison to the measured densities and suggested X-ray structures, a structure for the resting S_1-state is needed. Electrons and protons were therefore added to the S_4 structure until the S_1-state was reached. This structure, for the largest model used so far with about 190 atoms, is shown in Fig. 12, illustrating the size of the model and the amino acids included in the model.

The optimized structure for the S_1-state is also shown in Fig. 13, where the X-ray density from the London measurement is included. As seen in this figure, the structure fits very well into the density. It should

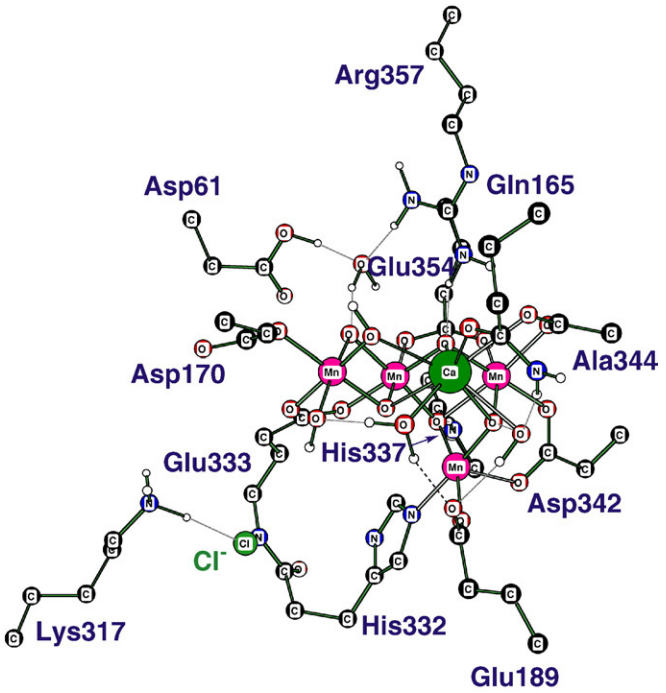

Fig. 12. The largest model used to study water oxidation. The structure is for the S_1-state and has been fully optimized. Most amino acid protons have been left out.

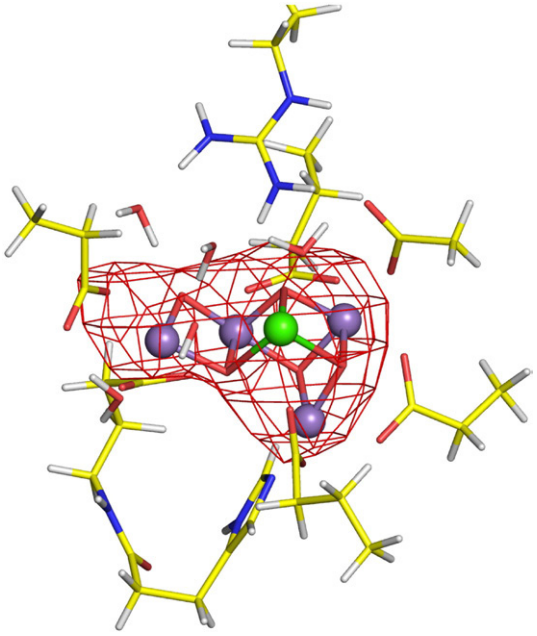

Fig. 13. The DFT optimized S_1 structure placed into the X-ray density from the London X-ray measurements.

again be emphasized that the structure was not fitted to the density but was optimized only with the constraints of fixed backbone atoms. There are rather clear differences between the optimized metal positions and those obtained from the X-ray analysis. The deviations between the calculated positions and those suggested from the London X-ray study are between 0.6 and 1.5 Å. For the Berlin structure, the corresponding deviations are between 0.1 and 1.8 Å. This illustrates the problem with the low resolution, since all three complexes fit well into the density. However, it should also be noted that the effect of X-ray reduction on the density is not noticeable at this resolution since the DFT optimized structure, which is not reduced, still fits the density.

An interesting aspect of the DFT structure is that it has clear similarities to structures suggested by EXAFS studies [51,52], where it had been emphasized that substantial discrepancies exist between EXAFS and X-ray structures. One characteristic feature of the suggested EXAFS structures is that there should be a short Mn–Mn distance between the outer manganese and the nearest manganese in the Mn_3Ca-cube. These manganese atoms should therefore be connected by two μ-oxo bonds. This is precisely what is found in the optimized structure in Fig. 13. In contrast, in the London X-ray structure, the outer manganese is connected directly to one of the bridging oxo-ligands in the Mn_3Ca-cube, while in the Berlin structure, it is connected only by a single oxo-bond.

The number of short Mn–Mn distances in the S_1-state has been a controversial issue with different suggestions. The best optimized structure at present has Mn–Mn distances of 2.73, 2.86, 2.88 and 3.11 Å. This is in as good agreement with EXAFS suggestions as one can hope for using DFT. In one EXAFS interpretation [51], three distances of 2.7–2.8 Å and one of 3.3 Å are suggested, while in another one only two short 2.7 Å distances are suggested [52], illustrating the remaining EXAFS uncertainties.

With the two assumptions described above, that the backbone atoms are reasonably well positioned from the X-ray analysis, and that the lowest energy structure with constrained backbone atoms is the one that the enzyme adopts, it is thus claimed that the structure in Fig. 13 should be close to the actual OEC. It is interesting to compare this structure to other ones that have been suggested based on other DFT approaches. Two criteria will be used, the lowest energy and the fit to the protein structure. The first comparison will be to the structure

obtained by the QM/MM approach mentioned above [46]. Since that structure was obtained in an optimization for the full protein, it is clear that it fits the protein structure well. The same can be said about the present structure, where the backbone atoms were taken directly from the protein. It remains to compare the energies of the OEC clusters obtained with the two approaches. To do this, a model needs to be constructed for the two structures with the same number of atoms and the same charge, which requires minor compromises. The choice made was a model with 142 atoms and a charge of +2. It contains all the amino acids mentioned above. The backbone atoms were fixed, either from the X-ray analysis for the present structure or from the QM/MM optimization for the other structure. The charge of +2 is optimal for the 142 atom model of the QM/MM structure but the present structure should ideally have a charge of −1. Three protons were therefore added to reach a charge of +2 also for this structure. Optimizing both these structures led to an energy difference of 71 kcal/mol in favor of the present structure. Since an energy difference of 5–10 kcal/mol should be enough to discriminate between two DFT structures, which do not differ in the oxidation states, it seems clear that the QM/MM structure can be ruled out as a candidate for the actual OEC. As stated above, it is in principle possible for an enzyme to adopt a structure which is not the lowest energy one, but in that case there must be barriers larger than 20–25 kcal/mol to prevent decay of the structure during the lifetime of the protein. To make sure that this is not the case, a beginning of a pathway for the decay of the 142 atom model of the QM/MM structure was also located. With barriers lower than 5 kcal/mol, the structure will decay in less than a nano-second following the pathway found, to another structure with 20 kcal/mol lower energy. From this point, it will most probably decay further, but this was not investigated. It is worth noting that even though the QM/MM structure can be ruled out by the calculations, it still matches many experimental spectral features, such as those from polarized EXAFS [53].

The obvious question arises of how it is possible that the same type of DFT calculations can give such drastically different answers. The reason is that there exist very many local minima for every structure of a large molecule, sometimes separated by rather small barriers. The optimization procedure is constructed in a way that the nearest local minimum from the starting point is the one that is normally obtained. Therefore, many quite different starting points have to be constructed to be certain that the resulting energy is at least reasonably close to the global minimum.

A quite different approach for obtaining improved structures from DFT has been used in a recent study [54]. Ten different models were constructed based on the core topology derived by polarized EXAFS spectra [42], and with a ligand structure chosen to fit reasonably well into the Berlin X-ray structure. These 10 structures were complemented by two structures obtained by the present DFT cluster approach. For these 12 structures, exchange coupling constants were determined by DFT calculations. A complete spectrum of magnetic sublevels could then be compared to experimental measurements by EPR and ENDOR. Based on the agreement with experiments, three of the structures were selected as the best candidates for the actual structure of the OEC.

In the same way as described above for the QM/MM structure, the 10 EXAFS structures have now been compared energetically to the best structure from the present DFT cluster approach. Again, clusters with the same charge and number of atoms as the 10 structures were constructed from the present structure and a comparison was made. It turned out that the 10 structures are between 34 and 63 kcal/mol higher in energy than the present structure and should therefore be safely ruled out as candidates for the OEC. The structures selected to be the best ones based on the spectroscopic comparison were 60 and 46 kcal/mol, respectively, higher in energy than the present one. It should be emphasized that the largest part of the energy difference to the present structure should come from the ligand arrangements. The metal core structure is less sensitive. Probably, this type of spectroscopic approach would therefore be more successful if the investigation was restricted to ligand structures which are low in energy. The difficulty to obtain reliable enough theoretical spectra based on DFT should not be underestimated either.

3.2. Mechanism and energetics for water oxidation

As described in the Energetics of the catalytic cycle in cytochrome oxidase section, it is relatively easy to set up part of an energy diagram for processes where electrons and protons are added or removed [26]. By removing both an electron and a proton (a hydrogen atom) simultaneously from the OEC, quite reliable energies for every second level can be obtained by calculating only relative H-atom binding energies. In contrast to the case where only a proton (pK_a value) or only an electron (redox potential) is removed, the effect of the protein surrounding is usually rather small. To construct the energy diagram for every second level from the calculated relative H-atom binding energies, the driving force for the full process is also needed. With the redox potential for the electron acceptor P^+_{680} of 1.25 V [55,56] and for oxygen of 0.8 V, the driving force for water oxidation becomes 41.5 kcal/mol. To obtain the full diagram, including also pK_a and redox potentials, a single parameter, obtained by minimizing the barriers, is required.

The energy diagram obtained using a slightly smaller model than the one in Fig. 12 with about 170 atoms is shown in Fig. 14. This model lacks the chloride and Lys317. S_n^m means that n is the number of the S-state and m is the charge of the complex (only including direct ligands to the OEC). The diagram obtained with a full membrane gradient is

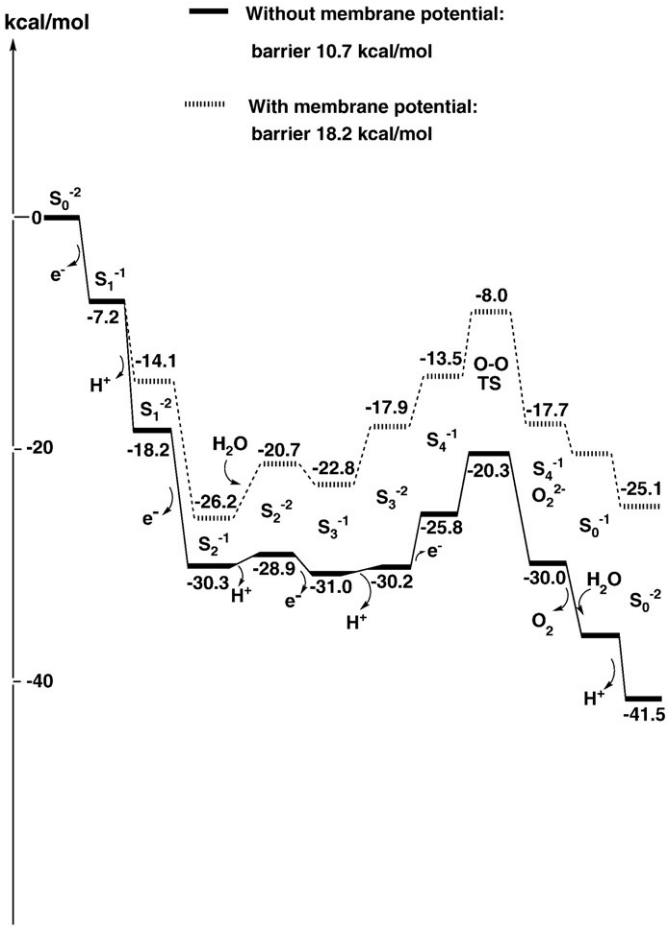

Fig. 14. Energy diagrams for dioxygen formation in PSII, with and without membrane gradient.

also shown in the figure. This diagram was obtained by adding a cost of 3 pK_a units (4.1 kcal/mol) every time a proton is released to the bulk.

The general shape of the energy diagram (without the membrane gradient) can be described as follows. The first two S-transitions are quite exergonic. The third one from S_2 to S_3 is obtained as almost thermoneutral but should be slightly exergonic. The formation of the oxygen radical in S_4 is endergonic by 5.2 kcal/mol and the local O–O formation barrier is 5.5 kcal/mol. This means that the total barrier for O–O bond formation is 10.7 kcal/mol, which is consistent with a process that takes milliseconds. The transition from S_3 to S_0 is exergonic by 11.3 kcal/mol.

The barrier obtained for the case with a membrane gradient is 18.2 kcal/mol (with respect to the S_2-state), which is somewhat too large compared to what can be expected from experiments. However, with respect to the S_3 state, the barrier is only 14.8 kcal/mol. The low energy for the S_2 state must be regarded as an error since this state should not be lower than the S_3-state even with membrane gradient. The error of a few kcal/mol is tolerable with respect to errors that have to be expected with the present methods. However, this error could also be an indication of a minor remaining problem with the chemical model used. An interesting aspect of the energy diagrams is that as much as 25 kcal/mol is wasted as heat for every O_2 molecule produced even with a maximal gradient. This is more than half of the energy available after the charge separation in the reaction center. The reason so much energy is lost is, of course, to increase the rate of the process.

The low barrier obtained with the mechanism described in Figs. 10 and 11 should be contrasted with the one obtained from the QM/MM study [46]. In that mechanism, an outside water reacts with the oxygen radical. For some models, these two mechanisms have been directly compared [47,50], and the latter mechanism was found to have a barrier sometimes (slightly dependent on the model) more than 20 kcal/mol higher than the one for the present mechanism.

The structural models obtained for the S-transitions are shown schematically in Fig. 15. The structures are taken from the optimizations but with all amino acids removed from the figure for clarity. The starting point S'_0 is a state where O_2 has just been removed in the previous cycle. When O_2 is removed, there is a relatively large opening in the middle of the OEC where the first water substrate can be bound. It binds with a simultaneous loss of a proton to the bulk. The product is shown as S_0, where an arrow indicates the position of the substrate OH. In the S_0 to S_1 transition, an electron is removed

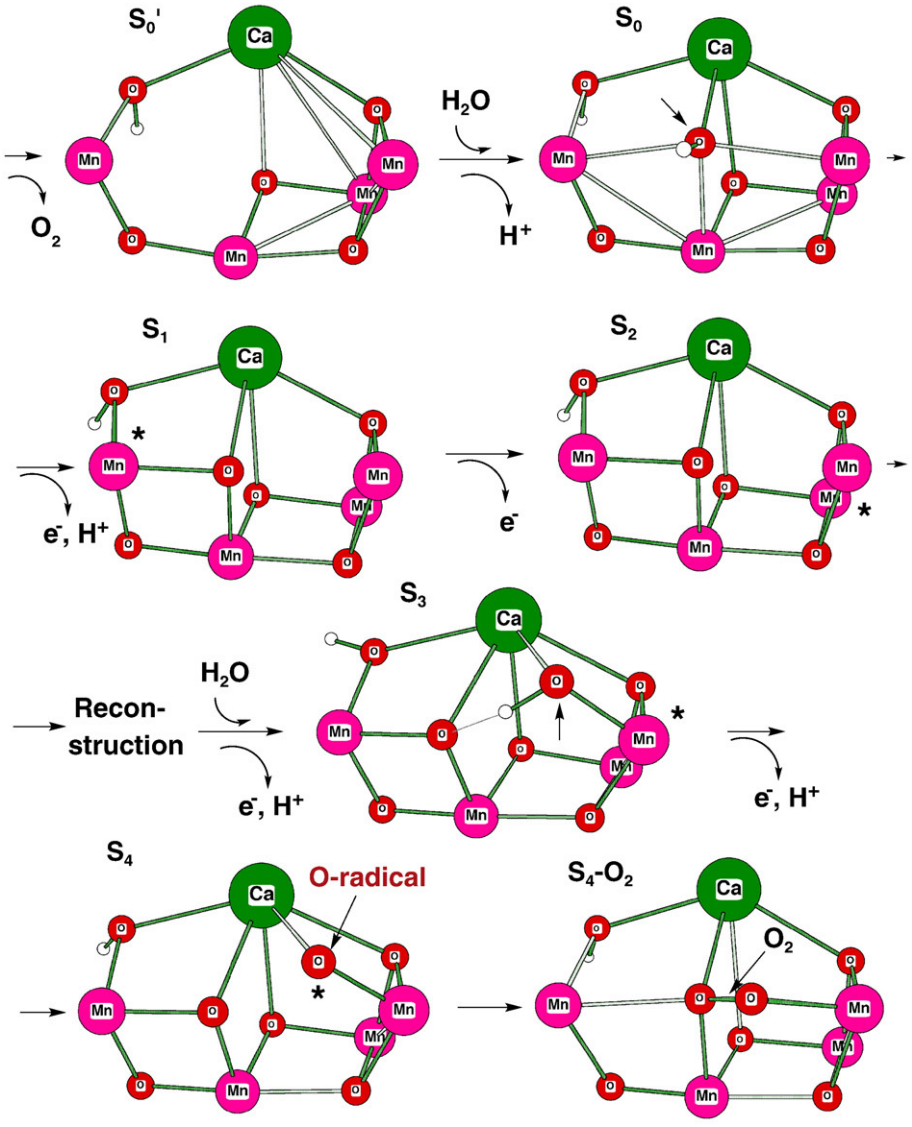

Fig. 15. Schematic picture of the different S-transitions. The structures have been optimized but only the most important atoms are shown. An asterisk (*) marks the atom that has been oxidized in that transition.

from the outer manganese (an asterisk (*) marks the oxidation in S_1) and a proton is released to the bulk. The proton is taken from the substrate OH. In the S_1 to S_2 transition, only an electron is removed in agreement with experiments [57-59]. The electron is taken from the manganese that binds Ala344. In the S_2 to S_3 transition, the next substrate water binds leading to a reconstruction, observed experimentally mainly by EXAFS [60,61]. The reconstruction occurs partly because there is not quite enough space for this water. A proton is simultaneously removed from the substrate water, exactly as in the formation of S_0, and an electron is taken from the manganese that binds His332. In the S_3-state, all manganese are Mn(IV). In the final transition from S_3 to S_4, a proton is taken from the substrate OH and an electron from the substrate oxygen. Finally, the O–O bond is formed between the oxygen radical and the oxo-group remaining from the first substrate water, O_2 is released, and the cycle starts all over again. The structures show that the OEC forms a basin where the two substrate waters can naturally fit and be deprotonated, without much occurring in the rest of the complex.

4. Concluding remarks

Quantum chemical high-accuracy DFT methods have been used to study problems in bioenergetics for a about a decade. During this time, the models have been gradually extended from about 30 atoms to more than 200 atoms, as commonly used today. This has led to a much higher level of understanding of advantages and limitations of this type of approach. A major step, taken recently, has been the ability to follow the convergence of the cluster model size all the way to quantitative convergence [62,63,45]. On the purely methodological side, the understanding of the density functionals has led to possibilities to better predict the accuracy for a given problem by varying the amount of exact exchange.

The present review has focused on the two main areas of bioenergetics, respiration and photosynthesis, in particular, the description and understanding of oxygen reduction and proton pumping in cytochrome oxidase, and water oxidation in photosystem II. The gradual increase of the understanding has been described. It is in this context important to realize that different models have during the years been used to study different aspects of the same enzyme. The different models used for water oxidation are illustrative. Five years ago, there was no X-ray structure of the oxygen evolving complex. The DFT studies at that time therefore had to focus on quite general aspects. Models of not more than 30–50 atoms that did not contain more than up to three manganese atoms may today appear as almost meaningless in their simplicity. Still, with these models, it could be shown that a low-barrier O–O bond formation will require a preformed oxygen radical [43,44], a finding that still holds today. To discuss and possibly improve the *structure* of the OEC, much more advanced models are now used. It has been argued here that a better structure than the ones directly deduced from X-ray analysis can be obtained by a careful combination of limited X-ray structural information and DFT optimizations. This has led to structural models which are in line with most experimental structural and spectroscopic findings. The energy diagram is also quite reasonable with a quite low barrier for O–O bond formation.

The quantum chemical modeling of different parts of the mechanism of cytochrome oxidase has been at least as demanding as the one for photosystem II. It has now, for example, been realized that in order to get a consistent picture of proton pumping from calculations, the direct use of experimental energetic information is necessary, in particular from rate measurements [12]. With a theoretical analysis combined with these measurements, a new picture for proton pumping has been achieved [11,13], see Fig. 4. A quite simple pictorial view is given for the most difficult part of the proton pumping process, the one which allows protons to be pumped against the gradient from the pump-loading site and not be allowed to go back to the N-side. It is shown that a coupling between an electron on heme a and a positive charge in the transition state region for proton transfer is required for gating. For oxygen reduction, the computational modeling has reached far but there are still major difficulties remaining. To understand how the reductive cycle can pump as many protons as the oxidative one will probably require new aspects of the models not yet accounted for.

References

[1] M.R.A. Blomberg, P.E.M. Siegbahn, G.T. Babcock, M. Wikström, O–O bond splitting mechanism in cytochrome c oxidase, J. Inorg. Biochemistry 80 (2000) 261–269.
[2] M.R.A. Blomberg, P.E.M. Siegbahn, G.T. Babcock, M. Wikström, Modeling cytochrome oxidase—a quantum chemical study of the O–O bond cleavage mechanism, J. Am. Chem. Soc. 122 (2000) 12848–12858.
[3] M. Karpefors, P. Ädelroth, A. Namslauer, Y. Zhen, P. Brzezinski, Formation of the "peroxy" intermediate in cytochrome *c* oxidase is associated with internal proton/hydrogen transfer, Biochemistry 39 (2000) 14664–14669.
[4] M.R.A. Blomberg, P.E.M. Siegbahn, M. Wikström, A metal-bridging mechanism for O–O bond cleavage in cytochrome *c* oxidase, Inorg. Chem. 42 (2003) 5231–5243.
[5] M.R.A. Blomberg, P.E.M. Siegbahn, Quantum chemistry applied to the mechanisms of transition metal containing enzymes—cytochrome *c* oxidase a particularly challenging case, J. Comp. Chem. 27 (2006) 1373–1384.
[6] P.E.M. Siegbahn, M.R.A. Blomberg, The Combined Picture from Theory and Experiments on Water Oxidation, Oxygen Reduction and Proton Pumping, Dalton Trans., 2009, pp. 5832–5840.
[7] L. Qin, J. Liu, D.A. Mills, D.A. Proshlyakov, C. Hiser, S. Ferguson-Miller, Redox-dependent conformational changes in cytochrome *c* oxidase suggest a gating mechanism for proton uptake, Biochemistry 48 (2009) 5121–5130.
[8] A. Kannt, R.D. Lancaster, H. Michel, The coupling of electron transfer and proton translocation: electrostatic calculations on *Paracoccus denitrificans* cytochrome *c* oxidase, Biophys. J. 74 (1998) 708–721.
[9] Y. Song, E. Michonova-Alexova, M.R. Gunner, Calculated proton uptake on anaerobic reduction of cytochrome *c* oxidase: is the reaction electroneutral? Biochemistry 45 (2006) 7959–7975.
[10] M. Bra(nden, H. Sigurdson, A. Namslauer, R.G. Gennis, P. A(delroth, P. Brzezinski, On the role of the K-proton transfer pathway in cytochrome *c* oxidase, Proc. Natl. Acad. Sci. USA 98 (2001) 5013–5018.
[11] P.E.M. Siegbahn, M.R.A. Blomberg, On the proton pumping mechanism in cytochrome *c* oxidase, J. Phys. Chem A 112 (2008) 12772–12780.
[12] I. Belevich, D.A. Bloch, N. Belevich, M. Wikström, M.I. Verkhovsky, Exploring the proton pump mechanism of cytochrome *c* oxidase in real time, Proc. Natl. Acad. Sci. USA 104 (2007) 2685–2690.
[13] P.E.M. Siegbahn, M.R.A. Blomberg, Energy diagrams and mechanism for proton pumping in cytochrome *c* oxidase, Biochim. Biophys. Acta 1767 (2007) 1143–1156.
[14] V.R.I. Kaila, M. Verkhovsky, G. Hummer, M. Wikström, Prevention of leak in the proton pump of cytochrome *c* oxidase, Biochim. Biophys. Acta 1777 (2008) 890–892.
[15] M. Wikström, M.I. Verkhovsky, G. Hummer, Water-gated mechanism of proton translocation by cytochrome *c* oxidase, Biochim. Biophys. Acta 1604 (2003) 61–65.
[16] Y.C. Kim, M. Wikström, G. Hummer, Kinetic gating of the proton pump in cytochrome *c* oxidase, Proc.Natl. Acad. Sci. USA 105 (2008) 6255–6259.
[17] V.R.I. Kaila, M. Verkhovsky, G. Hummer, M. Wikström, Glutamic acid 242 is a valve in the proton pump of cytochrome *c* oxidase, Proc. Natl. Acad. Sci. USA 105 (2008) 6255–6259.
[18] V.R.I. Kaila, M. Verkhovsky, G. Hummer, M. Wikström, Mechanism and energetics by which glutamic acid 242 prevents leaks in cytochrome *c* oxidase, Biochim. Biophys. Acta 1787 (2009) 1205–1214.
[19] D.M. Popovic, A.A. Stuchebrukhov, Proton pumping mechanism and catalytic cycle of cytochrome *c* oxidase: Coulomb pump model with kinetic gating, FEBS Lett 566 (2004) 126–130.
[20] E. Fadda, C.H. Yu, R. Pomes, Electrostatic control of proton pumping in cytochrome *c* oxidase, Biochim. Biophys. Acta 1777 (2008) 277–284.
[21] D.M. Popovic, J. Quenneville, A.A. Stuchebrukhov, DFT/electrostatic calculations of pK_a values in cytochrome *c* oxidase, J. Phys. Chem. B 109 (2005) 3616–3626.
[22] E. Fadda, N. Chakrabarti, R. Pomes, Acidity of a Cu-bound histidine in the binuclear center of cytochrome *c* oxidase, J. Phys. Chem. B 109 (2005) 22629–22640.
[23] D.V. Makhov, D.M. Popovic, A.A. Stuchebrukhov, Improved density functional theory/electrostatic calculation of the his291 protonation state in cytochrome *c* oxidase: self-consistent charges for solvation energy calculation, J. Phys. Chem. B 110 (2006) 12162–12166.
[24] P. Brzezinski, Redox-driven membrane-bound proton pumps, Trends Biochem. Sci. 29 (2004) 380–387.
[25] P.E.M. Siegbahn, M.R.A. Blomberg, M.L. Blomberg, A theoretical study of the energetics of proton pumping and oxygen reduction in cytochrome oxidase, J. Phys. Chem. B 107 (2003) 10946–10955.
[26] P.E.M. Siegbahn, M.R.A. Blomberg, in: K. Morokuma, J. Musaev (Eds.), Computational Modeling for Homogeneous Catalysis and Biocatalysis, Wiley-VCH, Germany, 2008, pp. 57–81.
[27] M. Wikström, Cytochrome *c* oxidase: 25 years of the elusive proton pump, Biochim. Biophys. Acta 1655 (2004) 241–247.
[28] M. Kaukonen, Calculated reaction cycle of cytochrome *c* oxidase, J. Phys. Chem. B 111 (2007) 12543–12550.

[29] J.A. Fee, D.A. Case, L. Noodleman, Toward a chemical mechanism of proton pumping by the b-type cytochrome *c* oxidase: application of density functional theory to cytochrome ba_3 of *Thermus thermophilus*, J. Am. Chem. 130 (2008) 15002–15021.
[30] D.B. Moore, T.J. Martinez, *Ab Initio* study of coupled electron transfer/proton transfer in cytochrome *c* oxidase, J. Phys. Chem. A 104 (2007) 2367–2374.
[31] D.A. Proshlyakov, T. Ogura, K. Shinzawa, S. Yoshikawa, T. Kitagawa, Resonance raman/absorption characterization of the oxo intermediates of cytochrome *c* oxidase generated in its reaction with hydrogen peroxide: pH and HO concentration dependence, Biochemistry 35 (1996) 8580–8586.
[32] M. Iwaki, A. Puustinen, M. Wikströmm, P.R. Rich, ATR-FTIR spectroscopy and isotope labeling of the p intermediate of *Paracoccus denitrificans* cytochrome *c* oxidase, Biochemistry 43 (2004) 14370–14378.
[33] V. Daskalakis, E. Pinakoulaki, S. Stavrakis, C. Varotis, Probing the environment of Cu_B in heme-copper oxidases, J. Phys. Chem. B 111 (2007) 10502–10509.
[34] A. Ghosh, A. Skancke, Revisiting the putative ferryl tilting mode of oxidized cytochrome *c* oxidase with density functional vibrational analysis of model complexes, J. Phys. Chem. B 102 (1998) 10087–10090.
[35] V. Daskalakis, S.C. Farantos, C. Varotis, Assigning vibrational spectra of ferryl-oxo intermediates of cytochrome *c* oxidase by periodic orbits and molecular dynamics, J. Am. Chem. Soc. 130 (2008) 12385–12393.
[36] S.B. Colbran, M.N. Paddo-Row, Could the tyrosine-histidine ligand to Cu_B in cytochrome *c* oxidase be coordinative labile? Implications from a quantum chemical model study of histidine substitutional lability and the effects of the covalent tyrosine–histidine crosslink, J. Biol. Inorg. Chem. 8 (2003) 855–865.
[37] V.R.I. Kaila, M.P. Johansson, D. Sundholm, L. Laakkonen, M. Wikström, The chemistry of the Cu_B site in cytochrome *c* oxidase and the importance of its unique His-Tyr bond, Biochim. Biophys. Acta 1787 (2009) 221–233.
[38] K. Kamiya, M. Boero, M. Tateno, K. Shiraishi, A. Oshiyama, Possible mechanism of proton transfer through peptide groups in the H-pathway of the bovine cytochrome *c* oxidase, J. Am. Chem. Soc. 129 (2007) 9663–9673.
[39] K.N. Ferreira, T.M. Iverson, K. Maghlaoui, J. Barber, S. Iwata, Architecture of the photosynthetic oxygen evolving center, Science 303 (2004) 1831–1838.
[40] B. Loll, J. Kern, W. Saenger, A. Zouni, J. Biesiadka, Towards complete cofactor arrangement in the 3.0 Å resolution structure of photosystem II, Nature 438 (2005) 1040–1044.
[41] A. Guskov, J. Kern, A. Gabdulkhakov, M. Broser, A. Zouni, W.J. Saenger, Location of chloride and its possible functions in oxygen-evolving photosystem II revealed by X-ray crystallography, Nat. Struct. Biol. 16 (2009) 334–341.
[42] J. Yano, J. Kern, K.D. Irrgang, M.J. Latimer, U. Bergmann, P. Glatzel, Y. Pushkar, J. Biesiadka, B. Loll, K. Sauer, J. Messinger, A. Zouni, V.K. Yachandra, X-ray damage to the Mn_4Ca complex in single crystals of photosystem II: a case study for metallo-protein crystallography, Proc. Natl. Acad. Sci. USA 102 (2005) 12047–12052.
[43] P.E.M. Siegbahn, R.H. Crabtree, Manganese oxyl radical intermediates and O–O bond formation in photosynthetic oxygen evolution and a proposed role for the calcium cofactor in photosystem II, J. Am. Chem. Soc. 121 (1999) 117–127.
[44] P.E.M. Siegbahn, Theoretical models for the oxygen radical mechanism of water oxidation and of the water oxidizing complex of photosystem II, Inorg. Chem. 39 (2000) 2923–2935.
[45] P.E.M. Siegbahn, F. Himo, Recent developments of the quantum chemical cluster approach for modeling enzyme reactions, J. Biol. Inorg. Chem. 14 (2009) 643–651.
[46] E.M. Sproviero, J.A. Gascon, J.P. McEvoy, G.W. Brudvig, V.S. Batista, QM/MM Models of the O_2-Evolving Complex of Photosystem II, J. Chem. Theor. Comput. 4 (2006) 1119–1134;
E.M. Sproviero, J.A. Gascon, J.P. McEvoy, G.W. Brudvig, V.S. Batista, Structural models of the oxygen-evolving complex of photosystem II, Curr. Opin. Struct. Biol. 17 (2007) 173–180;
E.M. Sproviero, K. Shinopoulos, J.A. Gascon, J.P. McEvoy, G.W. Brudvig, V.S. Batista, QM/MM computational studies of substrate water binding to the oxygen evolving complex of Photosystem II, Phil. Trans. R. Soc. B 363 (2008) 1149–1156;
E.M. Sproviero, J.A. Gascon, J.P. McEvoy, G.W. Brudvig, V.S. Batista, Quantum mechanics/molecular mechanics study of the catalytic cycle of water splitting in photosystem II, J. Am. Chem. Soc. 130 (2008) 3428–3442.
[47] P.E.M. Siegbahn, O–O bond formation in the S_4-state of the oxygen evolving center in photosystem II, Chem. Eur. J. 12 (2006) 9217–9227.
[48] P.E.M. Siegbahn, Water oxidation by the manganese cluster in photosynthesis, in: E.I Solomon, B. King, R. Scott (Eds.), Computational Inorganic and Bioinorganic Chemistry, John Wiley and Sons, Ltd, Chichester, England, 2009.
[49] P.E.M. Siegbahn, Structures and energetics for O_2 formation in photosystem II, Chem. Eur. J. 42 (2009) 1871–1880.
[50] P.E.M. Siegbahn, A structure consistent mechanism for dioxygen formation in photosystem II, Chem. Eur. J. 27 (2008) 8290–8302.
[51] J. Yano, J. Kern, K. Sauer, M.J. Latimer, Y. Pushkar, J. Biesiadka, B. Loll, W. Saenger, J. Messinger, A. Zouni, V.K. Yachandra, Where water is oxidized to dioxygen: structure of the photosynthetic Mn_4Ca Cluster, Science 314 (2006) 821–825;
J. Yano, J. Kern, Y. Pushkar, K. Sauer, P. Glatzel, U. Bergmann, J. Messinger, A. Zouni, Vs.K. Yachandra, High-resolution structure of the photosynthetic Mn_4Ca catalyst from X-ray spectroscopy, Phil. Trans. R. Soc. B 363 (2008) 1139–1147.
[52] H. Dau, A. Grundmeier, P. Loja, M. Haumann, On the structure of the manganese complex of photosystem II: extended-range EXAFS data and specific atomic-resolution models for four S-states, Phil. Trans. R. Soc. B 363 (2008) 1237–1244.
[53] E.M. Sproviero, J.A. Gascon, J.P. McEvoy, G.W. Brudvig, V.S. Batista, A model of the oxygen-evolving center of photosystem II predicted by structural refinement based on EXAFS simulations, J. Am. Chem. Soc. 130 (2008) 6728–6730.
[54] D.A. Pantazis, M. Orio, T. Petrenko, S. Zein, W. Lubitz, J. Messinger, F. Neese, Structure of the oxygen-evolving complex of photosystem II: information on the S_2 state through quantum chemical calculation of its magnetic properties, Phys. Chem. Chem. Phys. 11 (2009) 6788–6798.
[55] B.A. Diner, Amino acid residues involved in the coordination and assembly of the manganese cluster of photosystem II. Proton-coupled electron transport of the redox-active tyrosines and its relationship to water oxidation, Biochim, Biophys. Acta 1503 (2001) 147–163.
[56] F. Rappaport, J. Lavergne, Coupling of electron and proton transfer in the photosynthetic water oxidase, Biochim. Biophys. Acta 1503 (2001) 246–259.
[57] C.F. Fowler, Proton evolution from photosystem II. Stoichiometry and mechanistic considerations, Biochim. Biophys. Acta 462 (1997) 414–421.
[58] S. Saphon, A.R. Crofts, Protolytic reactions in photosystem II: a new model for the release of protons accompanying the photooxidation of water, Z. Naturforsch. 32C (1977) 617–626.
[59] V. Förster, W. Junge, Stoichiometry and kinetics of proton release upon photosynthetic water oxidation, Photochem. Photobiol. 41 (1985) 183–190.
[60] W. Liang, T.A. Roelofs, R.M. Cinco, A. Rompel, M.J. Latimer, W.O. Yu, K. Sauer, M.P. Klein, V.K. Yachandra, Structural change of the Mn cluster during the S_2 to S_3 state transition of the oxygen-evolving complex of photosystem II. Does it reflect the onset of water/substrate oxidation? Determination by Mn X-ray absorption spectroscopy, J. Am. Chem. Soc. 122 (2000) 3399–3412.
[61] M. Haumann, C. Muller, P. Liebisch, L. Iuzzolino, J. Dittmer, M. Grabolle, T. Neisius, W. Meyer-Klaucke, H. Dau, Structural and oxidation state changes of the photosystem II manganese complex in four transitions of the water oxidation cycle (S_0 to S_1, S_1 to S_2, S_2 to S_3, and S_3, S_4 to S_0,) characterized by X-ray absorption spectroscopy at 20 K and room temperature, Biochemistry 44 (2005) 1894–1908.
[62] R. Sevastik, F. Himo, Quantum chemical modeling of enzymatic reactions: the case of 4-oxalocrotonate tautomerase, Bioorg. Chem. 35 (2007) 444–457.
[63] K.H. Hopmann, F. Himo, Quantum chemical modeling of the dehalogenation reaction of haloalcohol dehalogenase, J. Chem. Theor. Comp. 4 (2008) 1129–1137.